5.1. Purification of BNCs by ultracentrifugation (≤10 mg protein per lot)

BNC and ZZ–BNC can be readily purified by ultracentrifugation owing to the overexpression of BNCs in yeast cells. The yeast cells (about 20 g wet weight) are disrupted with glass beads (0.5 mm in diameter, 175 ml) using a BEAD-BEATER (BioSpec Products, Bartlesville, OK, USA) in 160 ml of 0.1 *M* sodium phosphate buffer (pH 7.2) containing 7.5 *M* urea, 15 m*M* ethylenediaminetetraacetic acid (EDTA), 4 m*M* phenylmethylsulfonyl fluoride (PMSF), 0.1 m*M* 4-amidinophenyl-methanesulfonyl fluoride (APMSF), and 0.1% (v/v) Tween 80. The crude extract obtained by centrifugation at 34,780×*g* at 4 °C for 30 min (about 6 g of protein) is mixed with PEG 6000 solution (15%, w/v at final concentration) to precipitate BNCs. The precipitants (about 3 g of protein) are subjected to CsCl isopycnic ultracentrifugation (10–40%, w/v) using an SW28 rotor (Beckman Coulter, Inc., Fullerton, CA, USA) at 24,000 rpm at room temperature for 15 h. Fractions containing BNCs are determined by sandwich enzyme-linked immunosorbent assay (ELISA) for BNC using an IMx HBsAg assay system (Abbott Laboratories, Abbott Park, IL, USA). Positive fractions are subjected twice to sucrose density gradient ultracentrifugation (10–50%, w/v) using an SW28 rotor at 24,000 rpm at room temperature for 15 h. Fractions containing BNCs are concentrated by ultrafiltration using an Amicon Ultra 100,000 NMWL (Millipore, Billerica, MA, USA) and subjected to a Sephacryl S-500 HR (GE Healthcare, Waukesha, WI, USA) gel-filtration column equilibrated with phosphate-buffered saline (PBS) containing 1 m*M* EDTA. The protein concentration of BNCs is measured by a bicinchoninic acid (BCA) assay kit (Sigma-Aldrich, St Louis, MO, USA) using bovine serum albumin (BSA) as a calibration standard. Approximately 10 mg (as a protein) of BNC is obtained from recombinant yeast cells grown in 2 l of culture medium (Yamada *et al.*, 2001).

5.2. Purification of BNCs using column chromatography

The ultracentrifugation step is rate-limiting, time-consuming, and produces a low yield, so obtaining >10 mg of BNC per lot in 1 week is difficult. Based on the heat stability of BNCs (Yamada *et al.*, 2001), a large amount of yeast crude extract can be processed immediately by heat treatment (Jung *et al.*, unpublished data). The crude extract of yeast cells is obtained by the method described earlier, and then dialyzed three times against PBS containing 1 m*M* EDTA at 4 °C for 2 h to remove urea. The crude extract (about 6 g of protein) is dispensed to 40-ml plastic tubes, incubated at 70 °C for 20 min, and then centrifuged at 34,780×*g* at 4 °C for 30 min to remove yeast-derived proteins. The supernatant (about 800 mg of protein) is subjected to a sulfate-cellulofine column (1.6 × 20 cm; Chisso Corp., Tokyo,

Japan) equilibrated with PBS containing 150 m*M* NaCl. After the stepwise elution of PBS containing 1 *M* NaCl, the fraction containing a BNC is concentrated by ultrafiltration using an Amicon Ultra 100,000 NMWL (about 120 mg of protein) and then subjected to a Sephacryl S-500 HR gel-filtration column (1.6 × 60 cm) equilibrated with PBS containing 1 m*M* EDTA. About 60 mg of the highly purified BNC is obtained from the yeast cells grown in 2 l of culture medium.

5.3. Purification of ZZ–BNC using column chromatography

Porcine IgG is precipitated from porcine serum (Sigma-Aldrich) with $(NH_4)_2SO_4$ (40% saturation), dissolved in PBS, and dialyzed against PBS at 4 °C for 48 h. The dialyzed solution is mixed with two-times volume of 60 m*M* acetate buffer (pH 4.8) and then mixed with *n*-caprylic acid to achieve a final concentration of 6.8% (v/v). After incubation at room temperature for 30 min with gentle stirring, the supernatant containing purified IgG is obtained by brief centrifugation. Purified porcine IgG is conjugated to an NHS-activated Sepharose 4B Fast Flow (GE Healthcare) column according to manufacturer's instructions. The IgG-conjugated Sepharose column is equilibrated with PBS.

Preparation of the crude extract of yeast and heat treatment are the same as the BNC protocol. The supernatant is subjected to the porcine IgG-conjugated Sepharose column (affinity chromatography) to capture ZZ–BNC specifically using the IgG–ZZ domain interaction. The column is washed extensively with 75 m*M* Tris–HCl (pH 7.2) containing 10 m*M* NaCl, and then ZZ–BNC is obtained by the stepwise elution of 10 m*M* Tris–HCl (pH 7.2) containing 3.5 *M* NaSCN, 500 m*M* NaCl, and 10 m*M* EDTA. Fractions containing ZZ–BNC are subjected to a Sephacryl S-500 HR gel-filtration column (1.6 × 60 cm) equilibrated with PBS containing 1 m*M* EDTA. About 30 mg of highly purified ZZ–BNC can be obtained from yeast cells grown in 2 l of culture medium.

6. Conjugation of BNCs with LPs

The LPs used for BNC conjugation (Fig. 8.2) can be prepared by conventional methods such as solvent evaporation (Bangham and Horne, 1964), ethanol injection (Batzri and Korn, 1973), and reverse-phase evaporation (Szoka and Papahadjopoulos, 1978). The lipid composition of LPs should be optimized for the materials to be incorporated, for example, cationic lipids for the preparation of DNA- or siRNA-containing LPs (i.e., lipoplexes; Chapter 14 of volume 465, Düzgüneş *et al.*, 2002; Li and Huang, 2006), and anionic/neutral lipids for chemical compounds

containing LPs. To our knowledge, all LPs that have been employed have resulted in the formation of BNC–LP conjugates.

6.1. Example 1.1: Preparation of BNC–LP conjugates containing DNA (BNC–lipoplex conjugates)

For preparation of a DNA–LP complex (lipoplex), we routinely use commercially available lyophilized cationic LPs containing *O,O'*-ditetradecanoyl-*N*-(α-trimethylammonioacetyl)diethanolamine chloride (DC-6-14; Kikuchi *et al.*, 1999) as the major cationic lipid, an essential component for the cellular uptake of DNA, for example, Coatsoame-EL-01-D (NOF, Tokyo, Japan) and LipoTrust series (Hokkaido System Science, Sapporo, Japan). In the case of Coatsome-EL-01-D, 1.5 mg of lyophilized LP (as lipids) is dissolved in 1 ml of 250 μg/ml luciferase (LUC) expression vector pGL3 (Promega, Madison, WI, USA) and incubated for 15 min to allow lipoplex formation. Aliquots of lipoplex (100 μg LP, 16.7 μg DNA) are mixed with freeze-dried BNC (100 μg as protein) and incubated at room temperature for 15 min. By changing the amount of LP used for 16.7 μg DNA, a series of lipoplex and BNC–lipoplex conjugates are prepared with an N/P ratio (molar ratio of nitrogen-atom content in cationic lipids to phosphorous-atom content in plasmid DNA) from 0.3 to 2.4. The z-averaged sizes and ζ-potentials of lipoplex and BNC–lipoplex conjugate are measured at 25 °C using a Zetasizer Nano-ZS (Malvern Instruments Ltd., Worcestershire, UK). When the content of cationic lipids in lipoplex is increased, z-averaged sizes and ζ-potentials are apt to increase to >1 μm and >0 mV, respectively, in accordance with the increase in N/P ratio (Fig. 8.3A). BNCs are found to keep the sizes of BNC–lipoplex conjugates to <200 nm and ζ-potentials negative.

6.2. Example 1.2: *In vitro* transfection with BNC–lipoplex conjugates

About 1×10^5 of human cells (hepatocarcinoma HepG2, colon carcinoma WiDr, cervical carcinoma HeLa) are seeded on a 24-well cell culture plate (Iwaki, Tokyo, Japan) and incubated for 24–48 h in a humidified atmosphere at 37 °C in 5% (v/v) CO_2. Aliquots of BNC–lipoplex conjugates containing pGL3 (N/P ratio = 1.4; 100 μg LP, 16.7 μg DNA, and 100 μg BNC (as protein)) are diluted with complete cell culture medium containing 10% (v/v) fetal bovine serum and antibiotics, and applied to each well with 1 μg/ml (as protein of BNC, 0.5 μg/well) at final concentration. The medium is exchanged after incubation for 3–6 h to avoid nonspecific cellular uptake, and then incubated for 48 h to allow LUC expression.

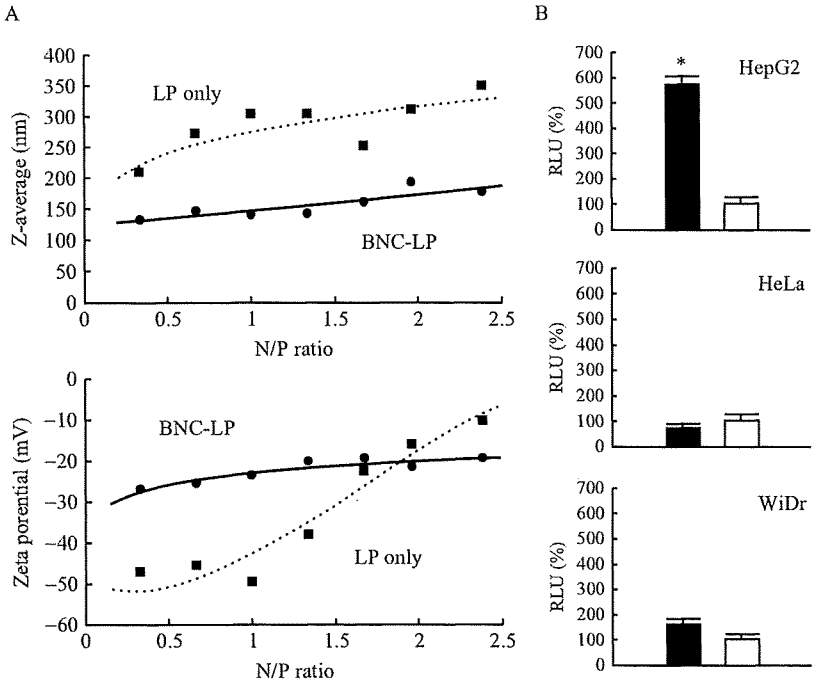

Figure 8.3 Effect of BNC conjugation on lipoplex (DNA-containing LPs). (A) *z*-averaged sizes (upper panel) and ζ-potentials (lower panel) of BNC–lipoplex conjugates (*circles* with *solid line*) and lipoplex (*squares* with *dashed line*) at the indicated N/P ratio. (B) *In vitro* transfection with LUC expression plasmid by BNC–lipoplex (*closed bars*) and lipoplex (*open bars*). LUC activities in cell lysates are measured 48 h after transfection. Mean ± S.D. ($n = 9$). $*p < 0.05$.

After lysis with passive lysis buffer (Luciferase Assay Kit, Promega), intracellular activities of LUC can be measured by a GloMax 20/20n Luminometer (Promega) using the LUC substrate luciferin. Human liver-derived HepG2 cells transfected with BNC–lipoplex conjugates containing pGL3 showed approximately five times higher LUC expression than those transfected with lipoplex containing pGL3, whereas human nonliver-derived HeLa cells and WiDr cells showed no significant differences in LUC expression between BNC–lipoplex conjugates and lipoplexes (Fig. 8.3B). These data indicated that the BNC–lipoplex conjugates deliver the LUC plasmid to human liver cells specifically *in vitro*. This prompted us to examine if BNC–lipoplex conjugates are more suitable than conventional lipoplexes for an *in vivo* pinpoint gene delivery system.

6.3. Example 1.3: *In vivo* transfection with BNC–lipoplex conjugates

Xenograft mouse models bearing tumors on their backs are generated using nude mice (5 weeks, male, BALB/c-nu/nu; CLEA Japan, Tokyo, Japan) under guidelines of the Institute of Scientific and Industrial Research, Osaka University, Japan. The cancer cell lines used are NuE and Huh-7 (human hepatocarcinoma), WiDr (human colon carcinoma), A431 (human epithelial carcinoma), PC12 (rat adrenal pheochromocytoma), and MDA-MB-435 (human breast carcinoma). About 1×10^6 cells are mixed with 50 μl of BD Matrigel Matrix HC (BD Biosciences, Bedford, MA, USA) and subcutaneously injected into the back of mice. After 2–4 weeks, mice possessing a tumor of appropriate diameter 1 cm can be obtained.

For the delivery of green fluorescent protein (GFP)-expression plasmid pEGFP-C1 (Clontech, Mountain View, CA, USA), BNC–lipoplex (N/P ratio = 1.4; 100 μg LP, 16.7 μg pEGFP-C1, and 100 μg BNC (as protein)) are intravenously injected to each tumor-bearing mouse. At 1 week after injection, mice are killed, and tumors and tissues (liver, lung, spleen, brain, heart, kidney) are isolated. Tissues and tumors are embedded in plastic resin or cryomold, cut into sections of 5 μm thickness, and observed using fluorescent microscopy or confocal laser scanning microscopy. GFP expression can be observed in only human liver-derived tumors, not in other tumors and tissues (Jung *et al.*, 2008).

6.4. Example 2.1: Preparation of BNC–LP conjugates containing DOX

Stock solutions of dipalmitoylphosphatidylcholine (DPPC, NOF), dipalmitoylphosphatidylethanolamine (DPPE, NOF), dipalmitoylphosphatidylglycerol sodium (DPPG-Na, NOF) are prepared in a chloroform/methanol (2:1, v/v) mixture at a concentration of 50 m*M*. A stock solution of cholesterol (Chol, NOF) is prepared in the same chloroform/methanol mixture at a concentration of 200 m*M*. All stock solutions are stored at −80 °C and prewarmed to 60 °C before use. Phospholipids and cholesterol (DPPC:DPPE:DPPG-Na:Chol = 15:15:30:40 molar ratio) are dissolved in the chloroform/methanol mixture in a round-bottomed flask, and then evaporated at 60 °C by utilizing a rotary evaporator to produce a thin hemispherical lipid film. The film is hydrated in buffer containing 10 m*M* HEPES (pH 4.0) and 120 m*M* $(NH_4)_2SO_4$ at 60 °C. The freeze–thaw cycle is repeated five times. The crude solution of LP is subjected to a Lipex extruder (Northern Lipids, Vancouver, BC, Canada) equipped with a polycarbonate filter (pore size, 200 nm) at 60 °C five times, followed by seven times with a filter (pore size, 50 nm). The *z*-average size of LP is

measured by dynamic light scattering at 25 °C using a Zetasizer Nano-ZS. The LPs are subjected to a Sephadex G-25 (GE Healthcare) gel-filtration column equilibrated with 10 m*M* HEPES buffer (pH 7.4) containing 100 m*M* NaCl and 3.4% (w/v) sucrose. Total lipid concentration is calculated from that of DPPC, which is determined by a Laboassay Phospholipid Kit (Wako, Osaka, Japan) utilizing choline oxidase and [*N*-ethyl-*N*-(2-hydroxy-3-sulfopropyl)-3,5-dimethoxyaniline] (DAOS) (Takayama *et al.*, 1977). To introduce DOX (also called adriamycin; Wako) into LPs by a remote-loading method, 200 μl of 10 mg/ml DOX–HCl solution is added to 15 mg of LP solution (as total lipids, prewarmed at 60 °C), and then incubated for 20 min at 60 °C with gentle stirring. After free DOX is removed by a Sephadex G-25 gel-filtration column, LPs containing DOX (about 2 mg DOX–HCl per 15 mg total lipid) can be obtained.

Aliquots of LPs containing DOX (2 mg LP, 0.27 mg DOX–HCl) are gradually added to freeze-dried BNC (100 μg as protein) and incubated at room temperature for 15 min to form a BNC–LP conjugate containing DOX. The diameter of the conjugate is estimated to be ~140 nm by the dynamic laser scattering method.

6.5. Example 2.2: *In vitro* cytotoxic effects of BNC–LP conjugates containing DOX

About 5×10^3 cells (HepG2, Huh-7, MDA-MB-435) cultured on a 96-well plate for 24–48 h are incubated with BNC–LP conjugates containing DOX at appropriate concentration (1–100 μg/ml as DOX) for 6–24 h and then incubated for 48–72 h in fresh complete medium. Cellular viability can be measured by the formation of formazan from a 3-(4,5-dimethylthiazol-2-yl)-2,5-diphenyltetrazolium bromide (MTT), a tetrazole probe using a CellTiter 96 Aqueous Non-Radioactive Cell Proliferation Assay (Promega). The strong cytotoxicity of BNC–LP conjugates containing DOX, comparable to that of DOX itself, can be observed in only human liver-derived HepG2 and Huh-7 cells, not in human nonliver-derived MDA-MB-435 cells (Fig. 8.4A). When comparing the cytotoxicity of BNC–LP conjugates with that of LP, BNC–LP conjugates showed strong cytotoxicity only toward HepG2 cells and Huh-7 cells, whereas LP did not show severe cytotoxicity to any cells. The half maximal inhibitory concentration (IC_{50}) of BNC–LP containing DOX for Huh-7 cells is 12 μg/ml, whereas that of LP containing DOX is 100 μg/ml. Doxil, a commercial PEGylated LP containing DOX (Markman, 2006), also showed a cytotoxicity curve similar to that of LP containing DOX. These data indicated that BNCs confer a human liver-specific active targeting function to LPs containing DOX.

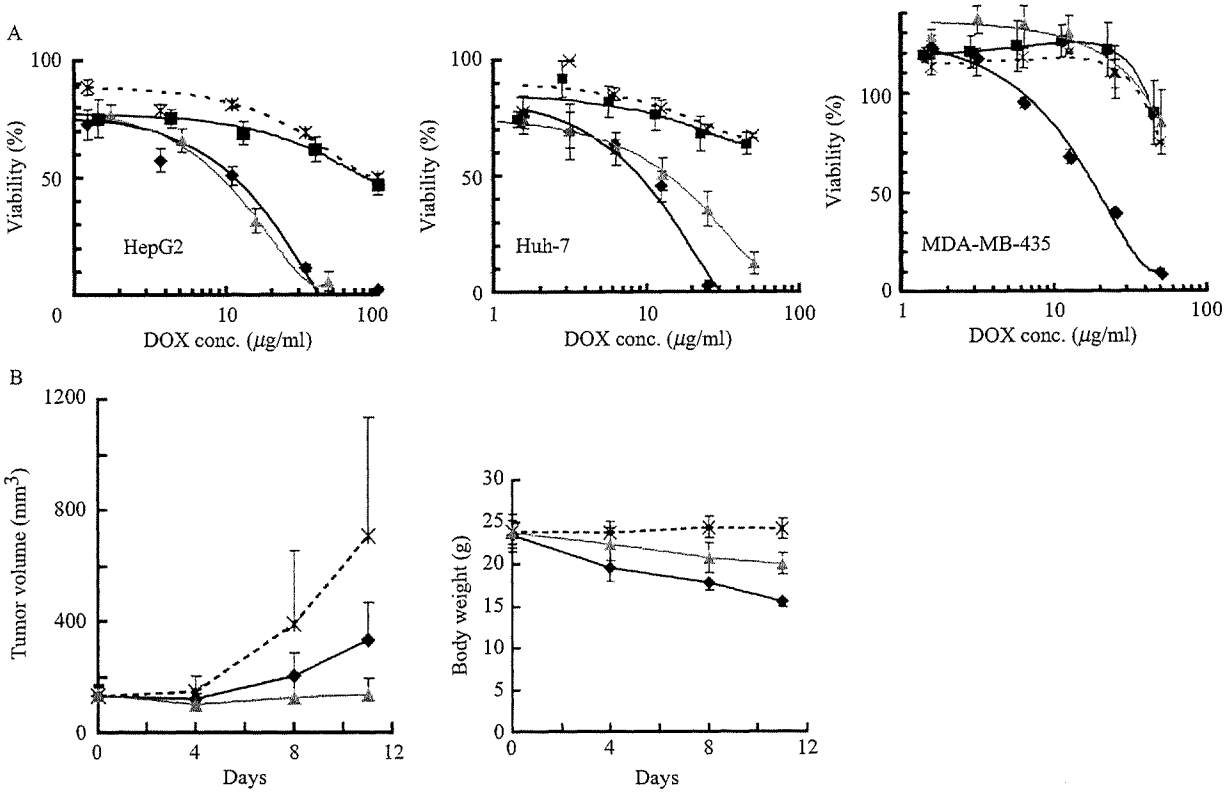

Figure 8.4 Effect of BNC conjugation on LP containing DOX. (A) *In vitro* cytotoxicity curves of BNC–LP conjugates. BNC–LP conjugates containing DOX (*triangles* with *gray lines*), LP containing DOX (*squares* with *solid lines*), DOX alone (*diamonds* with *solid lines*), and doxil (*crosses* with *dashed lines*). HepG2 cells (left panel), Huh-7 cells (center panel), and MDA-MB-435 cells (right panel). Mean ± SD ($n = 9$). (B) *In vivo* tumor suppression by BNC–LP conjugates. BNC–LP conjugates containing DOX (*triangles* with *gray lines*), DOX alone (*diamonds* with *solid lines*), and untreated control (*crosses* with *dashed lines*). Tumor volume (left panel) and body weight (right panel). Mean ± S.D. ($n = 9$).

6.6. Example 2.3: *In vivo* therapeutic effects of BNC–LP conjugates containing DOX

To the mouse xenograft model bearing Huh-7-derived tumors (about 1 cm in diameter), about 6 mg/kg (as DOX–HCl) of BNC–LP conjugates containing DOX is intravenously injected every 4 days under 10 ml/kg conditions. Largest (*a*) and smallest (*b*) superficial diameters of the tumor are measured every day, and tumor volume (V) is calculated as $V = ab^2/2$. BNC–LP conjugates containing DOX efficiently suppressed tumor growth, but identical amounts of DOX injected by LP only and injected alone failed to suppress it (Fig. 8.4B). As for toxicity, mice given about 8 mg/kg (as DOX–HCl) every 4 days by a BNC–LP conjugate showed less loss of body weight than those by DOX alone. A significant change in weight was not observed in tissues (liver, spleen, kidney, heart) 12 days after the first injection (data not shown). These data indicated that BNC–LP conjugates containing DOX possess not only active targeting machinery but also less toxicity.

When a mouse xenograft model bearing Huh-7-derived tumors received a single intravenous injection of BNC–LP conjugate containing DOX, LP containing DOX, doxil (PEGylated LP containing DOX), and DOX alone (8 mg/kg as DOX), blood is collected from the tail vein at 0, 30, 60, 120, and 180 min after the first injection. Plasma is collected by centrifugation at 3000 rpm at 4 °C, and DOX is extracted with a five volumes of the chloroform/methanol (4:1, v/v) mixture. After evaporation of solvent with nitrogen gas, the dried DOX fraction is subjected to high-performance liquid chromatography (HPLC) equipped with an octylsilanized gel column (Nucleosil 100 5C-18, Chemco Scientific Co. Ltd., Osaka, Japan) equilibrated with a 20 m*M* PBS/methanol mixture (25:75, v/v) containing 40 m*M* sodium heptane sulfonate. Flow rate is 1 ml/min, and DOX-derived fluorescence (excitation, 475 nm; emission, 554 nm) is determined using purified DOX as the internal standard. The initial concentration of DOX (0 min) in plasma is about 100 μg/ml in all mice (Fig. 8.5). The plasma concentration of DOX after 60 min in mice injected with a BNC–LP conjugate containing DOX is much higher than those with LP containing DOX and DOX alone, which is comparable to those with doxil. BNC conjugation, like PEGylation, enhances the robustness of LP against the RES.

7. Preparation of Antibody-Displaying BNC–LP Conjugates

ZZ–BNC–LP conjugates are prepared using ZZ–BNC instead of BNC by the method described earlier for *in vitro* and *in vivo* retargeting of BNC–LP conjugates according to antibody affinity. LP conjugation must

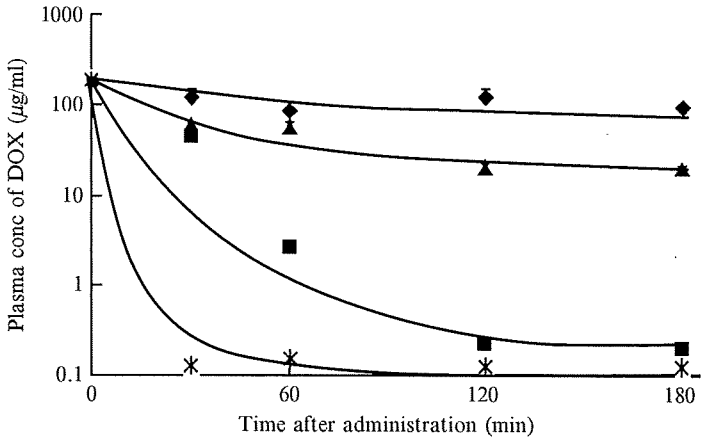

Figure 8.5 Plasma concentration of DOX. BNC–LP conjugates containing DOX (*triangles* with *solid line*), LP containing DOX (*squares* with *solid lines*), DOX alone (*crosses* with *solid lines*), and doxil (*diamonds* with *solid lines*).

be done before displaying antibodies on the surface of ZZ–BNC because antibodies displayed onto ZZ–BNC significantly reduce the fusogenic activity of ZZ–BNC (presumably by increased steric hindrance). Briefly, an aliquot of LPs (2 mg LP) containing materials of interest is gradually added to freeze-dried ZZ–BNC (100 μg as protein). We routinely add the smaller amount of antibody than ZZ–BNC (as protein) ranging from 1/5 to 1/100 (as protein) to the ZZ–BNC–LP solution. Antibodies may be spontaneously aligned on the surface of ZZ–BNC–LP conjugates by interaction of the IgG Fc domain with the ZZ domain. In the case of displaying IgG harboring weak affinity to the ZZ domain (Björck and Kronvall, 1984), a membrane-impermeable amine-reactive cross-linking agent such as bis(sulfosuccinimidyl)suberate (BS^3; Thermo Fisher Scientific, Waltham, MA, USA) was used to cross-link the binding between the IgG Fc domain and ZZ–BNC. Five millimolar BS^3 dissolved in dimethylsulfoxide (DMSO) is added to the ZZ–BNC–LP displaying IgG to a concentration of 50 μ*M*, allowed to react for 1 h, and free BS^3 removed by the reaction with 0.1 m*M* glycine. The antibody-displaying ZZ–BNC–LP conjugate is ready for *in vitro* and *in vivo* use. To our knowledge, it is not necessary to display the antibodies as much as possible onto ZZ-BNC for maximizing the delivering ability of ZZ-BNC-LP conjugate, strongly suggesting that the amounts of antibody on ZZ-BNC should be optimized in *in vitro* system.

8. Preparation of Biotin-Displaying BNC–LP Conjugates

For *in vitro* and *in vivo* retargeting of BNC–LP conjugates by various biorecognition molecules (e.g., cytokines, peptides, lectins, glycans), the surface of BNCs should be modified with these molecules without affecting fusogenic activity. The ZZ domain displayed on ZZ–BNC possesses many Lys residues, so the ε-amino residues are modified with biotin (the smallest high-affinity tag) using sulfo-biotin-NHS-ester (Thermo Fischer Scientific) according to the manufacturer's protocol. The number of biotins displayed on the surface of ZZ–BNC can be measured utilizing a 4′-hydroxyazobenzene-2-carboxylic acid (HABA) assay kit (Thermo Fisher Scientific). Usually, 1 mol of ZZ–BNC is modified with about 35 mol of biotin. Next, biotinylated ZZ–BNC–LP conjugate is mixed with an equimolar amount of biotinylated biorecognition molecules and avidins (e.g., avidin, streptavidin, neutravidin) to display the biorecognition molecules onto ZZ–BNC. As described in the antibody-displaying ZZ–BNC, the display of biorecognition molecules should be done after formation of the BNC–LP conjugate. The steric hindrance of biotinylated biorecognition molecules and avidins is too large for ZZ–BNC to exhibit fusogenic activity. The biorecognition molecules displaying the ZZ–BNC–LP conjugate is ready for *in vitro* and *in vivo* use. To our knowledge, it is not necessary to maximize the biorecognition molecules on ZZ–BNC to maximize the delivery capacity of the ZZ–BNC–LP conjugate, strongly suggesting that the amounts of biorecognition molecules on ZZ–BNC should be optimized in *in vitro* systems.

9. Concluding Remarks

The studies and methods described in this chapter demonstrate that the BNC–LP conjugate, as a hybrid of a viral vector and LPs, is a promising and rational approach to achieving a pinpoint delivery system for drugs and genes *in vivo*. Two major problems associated with BNC–LP conjugates must be resolved before they are in clinical use. The first problem is the immunogenicity of BNC–LP. BNC was initially developed as an immunogen of a recombinant hepatitis B vaccine, so BNC *per se* sometimes elicits an unexpected level of immune response. Recently, we succeeded in reducing the immunogenicity by incorporating HBV escape mutants, which can proliferate in humans vaccinated with hepatitis B vaccine. The second problem is the nonspecific incorporation by the RES. Like other nanoparticle-based medicines, BNC–LP conjugates cannot fully escape from the

RES, whereas HBV can accomplish the escape. We must analyze the endogenous escape mechanism of HBV at the molecular level, and introduce it to BNC–LP conjugates.

ACKNOWLEDGMENTS

The authors thank Professor M. Seno (Okayama University), Professor A. Kondo (Kobe University), and Professor M. Ueda (Keio University) for their helpful advice. We are grateful to Ms. Y. Matsushita, Ms. N. Shikaku, and Ms. Y. Matsui for their technical support. This work was supported in part by the Regional Research and Development Resources Utilization Program from the Japan Science and Technology Agency.

REFERENCES

Bangham, A. D., and Horne, R. W. (1964). Negative staining of phospholipids and their structural modification by surface-active agents as observed in the electron microscope. *J. Mol. Biol.* **8,** 660–668.

Batzri, S., and Korn, E. D. (1973). Single bilayer liposomes prepared without sonication. *Biochim. Biophys. Acta* **298,** 1015–1019.

Björck, L., and Kronvall, G. (1984). Purification and some properties of streptococcal protein G, a novel IgG-binding reagent. *J. Immunol.* **133,** 969–974.

Düzgüneş, N., Simões, S., Pires, P., and Pedroso de Lima, M. C. (2002). Gene delivery by cationic liposome-DNA complexes. *In* "Polymeric Biomaterials," (S. Dumitriu, ed.), pp. 943–958. Marcel Dekker, New York.

Glebe, D., and Urban, S. (2007). Viral and cellular determinants involved in hepadnaviral entry. *World J. Gastroenterol.* **13,** 22–38.

Hama, S., Akita, H., Ito, R., Mizuguchi, H., Hayakawa, T., and Harashima, H. (2006). Quantitative comparison of intracellular trafficking and nuclear transcription between adenoviral and lipoplex systems. *Mol. Ther.* **13,** 786–794.

Hinnen, A., Hicks, J. B., and Fink, G. R. (1978). Transformation of yeast. *Proc. Natl. Acad. Sci. USA* **75,** 1929–1933.

Hong, R. L., Huang, C. J., Tseng, Y. L., Pang, V. F., Chen, S. T., Liu, J. J., and Chang, F. H. (1999). Direct comparison of liposomal doxorubicin with or without polyethylene glycol coating in C-26 tumor-bearing mice: Is surface coating with polyethylene glycol beneficial? *Clin. Cancer Res.* **5,** 3645–3652.

Iwasaki, Y., Ueda, M., Yamada, T., Kondo, A., Seno, M., Tanizawa, K., Kuroda, S., Sakamoto, M., and Kitajima, M. (2007). Gene therapy of liver tumors with human liver-specific nanoparticles. *Cancer Gene Ther.* **14,** 74–81.

Jung, J., Matsuzaki, T., Tatematsu, K., Okajima, T., Tanizawa, K., and Kuroda, S. (2008). Bio-nanocapsule conjugated with liposomes for *in vivo* pinpoint delivery of various materials. *J. Control. Release* **126,** 255–264.

Kasuya, T., and Kuroda, S. (2009). Nanoparticles for human liver-specific drug and gene delivery systems: *In vitro* and *in vivo* advances. *Expert Opin. Drug Deliv.* **6,** 39–52.

Kasuya, T., Nomura, S., Matsuzaki, T., Jung, J., Yamada, T., Tatematsu, K., Okajima, T., Tanizawa, K., and Kuroda, S. (2008a). Expression of squamous cell carcinoma antigen-1 in liver enhances the uptake of hepatitis B virus envelope-derived bio-nanocapsules in transgenic rats. *FEBS J.* **275,** 5714–5724.

Kasuya, T., Yamada, T., Uyeda, A., Matsuzaki, T., Okajima, T., Tatematsu, K., Tanizawa, K., and Kuroda, S. (2008b). *In vivo* protein delivery to human liver-derived cells using hepatitis B virus envelope pre-S region. *J. Biosci. Bioeng.* **106,** 99–102.

Kasuya, T., Jung, J., Kadoya, H., Matsuzaki, T., Tatematsu, K., Okajima, T., Miyoshi, E., Tanizawa, K., and Kuroda, S. (2008c). *In vivo* delivery of bionanocapsules displaying *Phaseolus vulgaris* agglutinin-L_4 isolectin to malignant tumors overexpressing *N*-acetylglucosaminyltransferase V. *Hum. Gene Ther.* **19,** 887–895.

Kikuchi, A., Aoki, Y., Sugaya, S., Serikawa, T., Takakuwa, K., Tanaka, K., Suzuki, N., and Kikuchi, H. (1999). Development of novel cationic liposomes for efficient gene transfer into peritoneal disseminated tumor. *Hum. Gene Ther.* **10,** 947–955.

Kobayashi, M., Asano, T., Utsunomiya, M., Itoh, Y., Fujisawa, Y., Nishimura, O., Kato, K., and Kakinuma, A. (1988). Recombinant hepatitis B virus surface antigen carrying the pre-S2 region derived from yeast: Purification and characterization. *J. Biotechnol.* **8,** 1–22.

Kurata, N., Shishido, T., Muraoka, M., Tanaka, T., Ogino, C., Fukuda, H., and Kondo, A. (2008). Specific protein delivery to target cells by antibody-displaying bionanocapsules. *J. Biochem.* **144,** 701–707.

Kuroda, S., Otaka, S., Miyazaki, T., Nakao, M., and Fujisawa, Y. (1992). Hepatitis B virus envelope L protein particles. Synthesis and assembly in *Saccharomyces cerevisiae*, purification and characterization. *J. Biol. Chem.* **267,** 1953–1961.

Lasic, D., and Martin, F. (eds.) (1995). *In* "Stealth Liposomes", CRC Press, Boca Raton, FL.

Li, S. D., and Huang, L. (2006). Gene therapy progress and prospects: Non-viral gene therapy by systemic delivery. *Gene Ther.* **13,** 1313–1319.

Lorusso, V., Manzione, L., and Silvestris, N. (2007). Role of liposomal anthracyclines in breast cancer. *Ann. Oncol.* **18,** 70–73.

Maeda, H., Wu, J., Sawa, T., Matsumura, Y., and Hori, K. (2000). Tumor vascular permeability and the EPR effect in macromolecular therapeutics: A review. *J. Control. Release* **65,** 271–284.

Markman, M. (2006). Pegylated liposomal doxorubicin in the treatment of cancers of the breast and ovary. *Expert Opin. Pharmacother.* **7,** 1469–1474.

Marshall, E. (2002). Clinical research. Gene therapy a suspect in leukemia-like disease. *Science* **298,** 34–35.

Moghimi, S. M., and Szebeni, J. (2003). Stealth liposomes and long circulating nanoparticles: Critical issues in pharmacokinetics, opsonization and protein-binding properties. *Prog. Lipid Res.* **42,** 463–478.

Moghimi, S. M., Hunter, A. C., and Murray, J. C. (2001). Long-circulating and target-specific nanoparticles: Theory to practice. *Pharmacol. Rev.* **53,** 283–318.

Nagaoka, T., Fukuda, T., Yoshida, S., Nishimura, H., Yu, D., Kuroda, S., Tanizawa, K., Kondo, A., Ueda, M., Yamada, H., Tada, H., and Seno, M. (2007). Characterization of bio-nanocapsule as a transfer vector targeting human hepatocyte carcinoma by disulfide linkage modification. *J. Control. Release* **118,** 348–356.

Parr, M. J., Masin, D., Cullis, P. R., and Bally, M. B. (1997). Accumulation of liposomal lipid and encapsulated doxorubicin in murine Lewis lung carcinoma: the lack of beneficial effects by coating liposomes with poly(ethylene glycol). *J. Pharmacol. Exp. Ther.* **280,** 1319–1327.

Richardson, M. (2006). AmBisome: Adds to the body of knowledge and familiarity of use. *Acta Biomed.* **77,** 3–11.

Rosenthal, E., Poizot-Martin, I., Saint-Marc, T., Spano, J. P., and Cacoub, P.DNX Study Group (2002). Phase IV study of liposomal daunorubicin (DaunoXome) in AIDS-related Kaposi sarcoma. *Am. J. Clin. Oncol.* **25,** 57–59.

Savulescu, J. (2001). Harm, ethics committees and the gene therapy death. *J. Med. Ethics* **27,** 148–150.

Szoka, F. Jr., and Papahadjopoulos, D. (1978). Procedure for preparation of liposomes with large internal aqueous space and high capture by reverse-phase evaporation. *Proc. Natl. Acad. Sci. USA* **75,** 4194–4198.

Takayama, M., Itoh, S., Nagasaki, T., and Tanimizu, I. (1977). A new enzymatic method for determination of serum choline-containing phospholipids. *Clin. Chim. Acta* **79,** 93–98.

Tsutsui, Y., Tomizawa, K., Nagita, M., Michiue, H., Nishiki, T., Ohmori, I., Seno, M., and Matsui, H. (2007). Development of bionanocapsules targeting brain tumors. *J. Control. Release* **122,** 159–164.

Yamada, T., Iwabuki, H., Kanno, T., Tanaka, H., Kawai, T., Fukuda, H., Kondo, A., Seno, M., Tanizawa, K., and Kuroda, S. (2001). Physicochemical and immunological characterization of hepatitis B virus envelope particles exclusively consisting of the entire L (pre-S1 + pre-S2 + S) protein. *Vaccine* **19,** 3154–3163.

Yamada, T., Iwasaki, Y., Tada, H., Iwabuki, H., Chuah, M. K., VandenDriessche, T., Fukuda, H., Kondo, A., Ueda, M., Seno, M., Tanizawa, K., and Kuroda, S. (2003). Nanoparticles for the delivery of genes and drugs to human hepatocytes. *Nat. Biotechnol.* **21,** 885–890.

Yu, D., Amano, C., Fukuda, T., Yamada, T., Kuroda, S., Tanizawa, K., Kondo, A., Ueda, M., Yamada, H., Tada, H., and Seno, M. (2005). The specific delivery of proteins to human liver cells by engineered bio-nanocapsules. *FEBS J.* **272,** 3651–3660.

Integrin signal masks growth-promotion activity of HB-EGF in monolayer cell cultures

Hiroto Mizushima[1], Xiaobiao Wang[1], Shingo Miyamoto[2] and Eisuke Mekada[1,*]

[1]Department of Cell Biology, Research Institute for Microbial Diseases, Osaka University, 3-1 Yamadaoka, Suita, Osaka 565-0871, Japan
[2]Department of Obstetrics and Gynecology, School of Medicine, Fukuoka University, 7-45-1 Nanakuma, Fukuoka 814-0180, Japan
*Author for correspondence (emekada@biken.osaka-u.ac.jp)

Accepted 11 September 2009
Journal of Cell Science 122, 4277-4286 Published by The Company of Biologists 2009
doi:10.1242/jcs.054551

Summary

The extracellular environment and tissue architecture contribute to proper cell function and growth control. Cells growing in monolayers on standard polystyrene tissue culture plates differ in their shape, growth rate and response to external stimuli, compared with cells growing in vivo. Here, we showed that the EGFR (epidermal growth factor receptor) ligand heparin-binding EGF-like growth factor (HB-EGF) strongly stimulated cell growth in nude mice, but not in cells cultured in vitro. We explored the effects of HB-EGF on cell growth under various cell culture conditions and found that growth promotion by HB-EGF was needed in three-dimensional (3D) or two-dimensional (2D) culture systems in which cell-matrix adhesion was reduced. Under such conditions, cell growth was extremely suppressed in the absence of HB-EGF, but markedly potentiated in the presence of HB-EGF. When the integrin signal was reduced using antibodies or knockout of either integrin β1 or focal adhesion kinase (FAK), cells showed HB-EGF-dependent growth. We also showed that EGF, transforming growth factor-α (TGFα) or ligands of other receptor tyrosine kinases (RTKs) stimulated cell growth in 3D culture, but not in tissue culture plates. These results indicate that the integrin signal was sufficient to support cell growth in 2D tissue culture plates without addition of the growth factor, whereas stimulation by growth factors was clearly demonstrated in culture systems in which integrin signals were attenuated.

Supplementary material available online at
http://jcs.biologists.org/cgi/content/full/122/23/4277/DC1

Key words: EGFR, HB-EGF, Integrin, 3D culture

Introduction

Establishment of cell culture methods of mammalian cells stimulated revolutionary progress in biology and medicine, and has now become an essential technology in cell biology research. Mammalian cell culture is most commonly achieved by incubating cells with a defined nutrient medium supplemented with serum in tissue culture plates. Cells attach and adhere onto the flat surface of glass or plastic plates and grow two dimensionally, forming monolayer sheets. Although the standard cell culture system has provided us with fundamental knowledge of cell and gene functions, this system is not an accurate representation of the in vivo environment in which the cells originally exist (Lee et al., 2007; Schmeichel and Bissell, 2003; Yamada and Cukierman, 2007). Tissues and organs are three-dimensional (3D). Cells grown on flat tissue culture plates (TCPs) using standard cell culture methods differ from those growing in their natural environments in terms of their morphology, physicochemical properties of the substrate they attach to, and cell-cell and cell-matrix interactions. Thus, the behavior, growth and differentiation, as well as their response to internal and external signals, of cells grown in the standard cell culture environments are largely different to that of cells grown in vivo.

The EGFR-ligand system supports the proliferation, motility, differentiation and survival of various cell types, thereby contributing to the development, morphogenesis and maintenance of homeostasis in the body. The EGF-EGFR system also has a pivotal role in the progression and development of malignant tumor growth (Hynes and Lane, 2005; Normanno et al., 2006; Lynch et al., 2004; Paszek et al., 2005). Furthermore, the overexpression of EGFR ligands induces or enhances cell growth in nude mice (Miyamoto et al., 2004; Ongusaha et al., 2004; Wang et al., 2006; Normanno et al., 2006). However, in contrast to the marked effects of EGFR ligands on tumor cell growth in vivo, the growth-promoting properties of the EGFR ligands have not been well documented in most cell types using standard cell culture methods. Early studies indicated that EGF increased the lifetime, but not the growth rate, of primary keratinocytes in culture (Rheinwald and Green, 1977). Previous studies using normal keratinocytes, fibroblasts, breast cancer cells and neuroblastoma cells reported that EGFR ligands stimulated cell growth with a minimal increase in cell numbers (Hashimoto et al., 1994; Ho et al., 2005; Lembach, 1976; Osborne et al., 1980). Moreover, in some cases, EGFR ligands induced cell-cycle arrest or apoptosis (Cao et al., 2000; Fan et al., 1995). Even under serum-depleted conditions, the addition of growth factors to the cell culture medium resulted in only a slight growth promotion, if any. The lack of an appropriate in vitro culture system to demonstrate growth promotion by EGFR ligands posed a limitation in understanding the signaling mechanism and molecules responsible for the proliferating effect of these growth factors. The exceptions are the myeloid lineage cell lines 32D and Ba/F3. These cell lines, which normally grow in suspension in an interleukin-3-dependent manner, can proliferate specifically in response to EGFR ligands by expressing ectopic EGFR in the absence of interleukin-3, thus facilitating observation of its growth-promotion activity (Higashiyama et al., 1995; Iwamoto et al., 1999; Pierce et al., 1988; Yu et al., 2002). These findings suggest that cellular responses to EGFR ligands vary according to the cell culture conditions and cell systems used for the study. However, the reason

for this low potency of EGFR ligands in most cell types has not been investigated in much detail.

HB-EGF is an essential member of the EGFR ligands in vivo, which is synthesized as a transmembrane precursor protein (proHB-EGF) (Higashiyama et al., 1991). Its extracellular domain is then cleaved by proteases, via a so-called ectodomain-shedding mechanism, which yields a soluble mature growth factor (sHB-EGF), which is similar to other EGFR ligands (Goishi et al., 1995; Massagué and Pandiella, 1993). In the course of the present study, we found that HB-EGF did not promote the growth of ovarian cancer cell lines under standard monolayer cell culture conditions, although it enhanced the cell growth rates when the same cell lines were injected into nude mice. Thus, we focused on the growth-stimulatory effect of HB-EGF under various culture conditions and found that this effect of HB-EGF was not well documented in the standard monolayer culture. However, it was particularly observed in culture systems in which the integrin signal was attenuated. We also show that such culture conditions enable the observation of cell proliferation by EGF, TGFα or ligands of other receptor tyrosine kinases (RTKs). The results of the present study indicate why the growth-promotion activity of growth factors has thus far not been well documented in vitro.

Results

HB-EGF promotes cell growth in vivo but not in vitro

We previously reported that the tumorigenicity of the ovarian cancer cell lines SKOV3 and RMG-1 when injected into nude mice were strongly enhanced by exogenous expression of HB-EGF, whereas small-hairpin RNA-mediated knockdown of endogenous HB-EGF or administration of the HB-EGF-specific inhibitor CRM197 suppressed their tumorigenicities (Miyamoto et al., 2004). We confirmed the contribution of HB-EGF to SKOV3 cell growth in vivo by overexpression or knockdown experiments (Fig. 1A). Although the tumorigenic growth of xenografted cells might be affected by various host factors, the marked growth-promotion effect of HB-EGF in vivo led to the proposal that HB-EGF also contributes to SKOV3 cell growth in vitro. To test this hypothesis, we compared the growth rates of SKOV3 cells, HB-EGF-overexpressing SKOV3 (SKOV-HB) cells and HB-EGF-knockdown SKOV3 cells under monolayer culture conditions using standard polystyrene tissue culture plates (TCPs). Contrary to our expectation, no obvious differences in the growth rates between the parental and HB-EGF-overexpressing SKOV3 cells in TCPs were observed (Fig. 1A). Moreover, SKOV3 cells expressing small-hairpin RNAs specific for HB-EGF, which had lost their tumorigenicity, were able to grow almost as quickly as the parental cells in TCPs (Fig. 1A).

To further study the effects of HB-EGF on cell growth, we used BRL cells, which are originally non-tumorigenic and become tumorigenic upon HB-EGF overexpression (Wang et al., 2006). We established BRL cells overexpressing wild-type HB-EGF (BRL-HB) or an ectodomain-shedding deficient mutant HB-EGF (BRL-HBuc) (Miyamoto et al., 2004; Yamazaki et al., 2003), and compared their growth rates with that of mock virus-infected BRL cells (BRL-mock). Although BRL-HB and BRL-HBuc cells expressed comparable amounts of the HB-EGF precursor (proHB-EGF), the secretion of sHB-EGF by BRL-HBuc cells was significantly reduced compared with that of BRL-HB cells (supplementary material Fig. S1). When BRL-HB cells were subcutaneously injected into nude mice they formed tumors, as reported previously (Wang et al., 2006). However, neither BRL-HBuc cells nor BRL-mock cells formed tumors until 3 weeks after injection (Fig. 1B). Similarly to SKOV3 cells, these cells grew at comparable rates in TCPs (Fig. 1B). These results indicated that HB-EGF promotes the growth of non-tumorigenic cells in vivo in an ectodomain-shedding-dependent manner, although HB-EGF did not potentiate cell growth in cells grown using in vitro culture conditions.

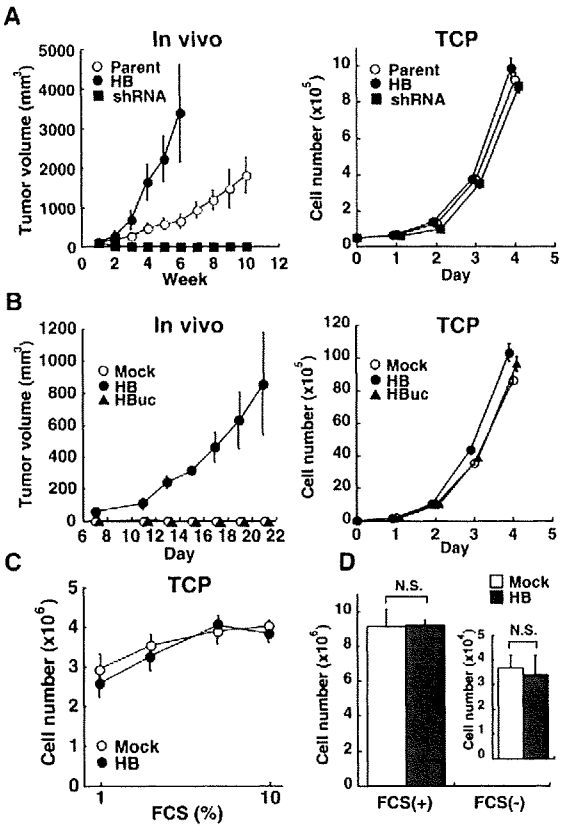

Fig. 1. Effects of HB-EGF on cell growth. (A) Tumorigenicity in vivo and growth of SKOV3 cells in TCPs. SKOV3 cells (Parent), SKOV3-HB cells (HB) or overexpressing small-hairpin RNAs for HB-EGF (shRNA) were injected into nude mice (n=16) or cultured in TCPs. The mean tumor volume (± s.d.) and cell number were determined. SKOV3 cells, SKOV-HB cells or SKOV3 cells expressing small-hairpin RNAs for HB-EGF were grown in TCPs. (B) Tumorigenicity in vivo and growth of BRL cells in TCPs. BRL cells (Mock), BRL-HB cells (HB) or BRL-HBuc cells (HBuc) were injected into nude mice (n=4) or cultured in TCPs. The mean tumor volume and cell number were determined. (C) Effect of FCS on BRL cell growth in TCPs. BRL cells (Mock) or BRL-HB cells (HB) were cultured with medium containing various concentrations of FCS for 4 days and cell number was counted. (D) Effects of HB-EGF on cell growth under FCS-free conditions. BRL cells (Mock) or BRL-HB cells (HB; 5×10^4) were cultured with FCS-containing or FCS-free defined medium for 4 days. Result for FCS-free defined medium is also shown in inset. N.S., not significant.

All the cultures described above were performed in medium containing 10% FCS. We tested the effect of serum on the growth-stimulating effect of HB-EGF in TCPs. Even in medium containing 1% FCS, the cells grew as quickly as those cultured in medium containing 10% serum; HB-EGF did not potentiate their growth rate (Fig. 1C). To rule out any effects of serum, cells were cultured using a serum-free defined medium as described in the Materials and Methods. Overall, the growth rate of BRL and SKOV3 cells,

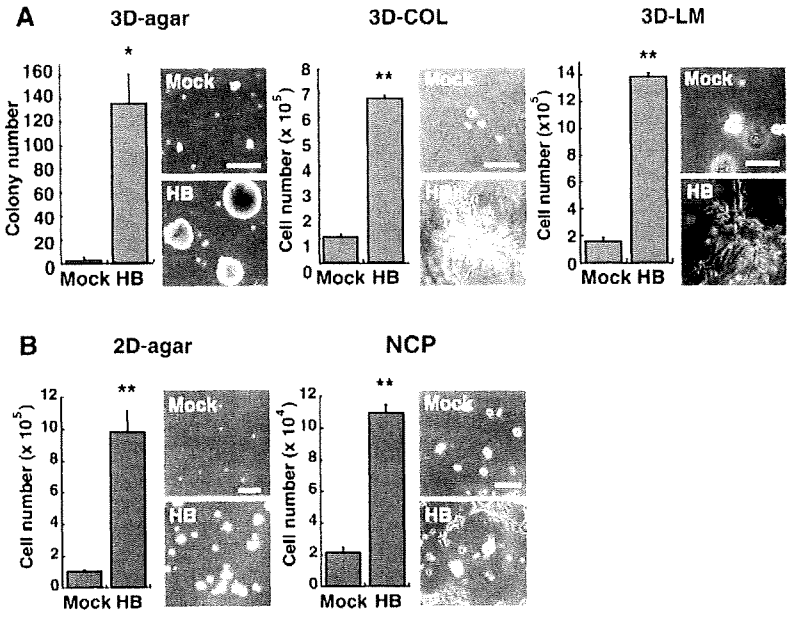

Fig. 2. Growth of BRL cells under various culture conditions. BRL cells (Mock) or BRL-HB cells (HB) were cultured under 3D culture conditions (A) or 2D culture conditions (B). (A) Cells were cultured in 3D-agar for 4 weeks, 3D-COL for 1 week or 3D-LM for 4 days. (B) Cells were cultured onto soft agar (2D-agar) for 1 week or NCPs for 3 days. Representative morphologies of BRL-mock and BRL-HB cells grown in 3D-agar (scale bar: 200 μm), 3D-COL (scale bar: 100 μm), 3D-LM (scale bar: 250 μm), 2D-agar (scale bar: 250 μm) or NCPs (scale bar: 250 μm) are shown. All cell cultures were maintained in the presence of FCS. *P<0.02, **P<0.01.

regardless of HB-EGF expression, was largely reduced under serum-free conditions. Even in the serum-free medium, HB-EGF did not enhance BRL (Fig. 1D) and SKOV3 cell growth (supplementary material Fig. S2).

To test whether the inability of HB-EGF to enhance cell growth in TCPs was a common feature, we tested the effect of HB-EGF on cell growth in three other cell lines, A431, RMG-1 and U373 MG cells. Similarly to BRL and SKOV3 cells, the exogenous expression of HB-EGF did not increase the growth rates of A431, RMG-1 and U373 MG cells in TCPs, either in medium containing 10% FCS or in serum-free defined medium (supplementary material Fig. S3). These results suggest that the inability of HB-EGF to promote growth in TCPs is not attributable to the existence of FCS in the culture medium.

HB-EGF enhances cell growth under 3D culture conditions

Tumorigenic cells can often grow in semisolid media, such as soft agar (Hanahan and Weinberg, 2000). HB-EGF induces oncogenic transformation in several cell lines and confers the ability to grow in soft agar (Fu et al., 1999; Harding et al., 1999; Ongusaha et al., 2004). Consistently with previous studies, HB-EGF strongly potentiated BRL cell growth in the presence of 10% FCS in soft agar (hereafter cell culture in soft agar is referred to as 3D-agar). BRL-HB cells grew to form spherical colonies in 3D-agar, but BRL-mock cells did not (Fig. 2A). One characteristic difference between cell culture conditions in 3D-agar and 2D plates is that cells embedded in gels grow three-dimensionally (in a multilayer). Therefore, we examined whether BRL cells grew in an HB-EGF-dependent manner under other 3D culture conditions. 3D cultures consisted of 3D matrices, such as collagen gels (hereafter referred to as 3D-COL) or a laminin-rich matrix (hereafter referred to as 3D-LM) (Paszek et al., 2005; Weaver et al., 1997). Although the morphology of BRL-HB cells growing in 3D-COL and 3D-LM was different to that in 3D-agar, HB-EGF markedly enhanced cell proliferation in these 3D cultures (Fig. 2A). In 3D-COL, BRL-mock cells proliferated to twice their initial number, whereas BRL-HB cells proliferated rapidly and increased their numbers around seven times faster than BRL-mock cells after 1 week of culture. BRL-HB cells proliferated even more rapidly in 3D-LM than in 3D-COL and multiplied around seven times faster than BRL-mock cells after 4 days of culture (Fig. 2A). Growth enhancement by HB-EGF in 3D culture conditions was observed for SKOV3, A431, RMG-1 and U373 MG cells (supplementary material Figs S2, S3).

In the above experiments, proHB-EGF was overexpressed in BRL cells and other cell lines to examine the effect of HB-EGF on cell growth. We also performed similar experiments by adding recombinant sHB-EGF to the medium as an alternative to proHB-EGF overexpression. sHB-EGF promoted the growth of BRL-mock cells in a dose-dependent manner in 3D-COL, but not in TCPs (supplementary material Fig. S4A). HB-EGF-dependent growth was also tested using MCF-10A, another non-transformed cell line. The addition of sHB-EGF induced a ~3.5-fold increase in growth of MCF-10A cells in 3D-LM, but weakly induced (~1.3-fold) growth of the cells in TCPs (supplementary material Fig. S4B). These results indicate that growth promotion by HB-EGF in 3D cultures is a general phenomenon observed for transformed and non-transformed cells, and that HB-EGF-dependent growth in 3D cultures is reflected by both the overexpression of proHB-EGF and by addition of sHB-EGF in the medium.

CRM197, a specific inhibitor of HB-EGF, suppresses HB-EGF-dependent growth of ovarian cancer cell lines in vivo (Miyamoto et al., 2004). CRM197 did not affect the growth of BRL-mock and BRL-HB cells in TCPs (supplementary material Fig. S5). In 3D-COL, however, CRM197 suppressed the growth of BRL-HB, but not BRL-mock cells, further confirming HB-EGF-dependent growth in 3D-COL (supplementary material Fig. S5).

HB-EGF enhances cell growth under 2D reduced cell adhesion conditions

As shown above, the growth enhancement by HB-EGF was clearly observed in 3D culture systems in which cells were embedded either into a soft agar, collagen or laminin-rich matrix. To determine whether the embedding of cells into the gel was critically required for cell growth enhancement by HB-EGF, we tested other cell

culture conditions: (1) cells were cultured atop a soft agar surface (2D-agar); (2) cells were cultured on NanoCulture® plates (NCPs). We compared the growth rate of BRL-HB cells with those of BRL-mock cells grown under these culture conditions. When BRL cells were cultured in 2D-agar, cell adhesion and spreading were strongly suppressed. Under these conditions, BRL-mock cells scarcely grew, but BRL-HB cells proliferated and formed spheroidal cell masses (Fig. 2B). NCPs with a nanometer scale honeycomb-patterned structure on the surface are shown to reduce cell adhesion to the matrix (http://www.scivax.com/cell/english/index.html). In NCPs, cell adhesion, spreading and monolayer cell sheet formation were hampered in the case of BRL cells, and these cells showed HB-EGF-dependent growth (Fig. 2B).

Cells embedded in gels might differ from cells growing in TCPs largely because of their surrounding microenvironments. In 3D, for example, gas exchange, nutrient supply and diffusion of growth factors might be hampered, compared with TCPs. However, since growth promotion by HB-EGF was observed to be as high as that of 3D culture conditions using 2D-agar or NCP, the difference of these factors might not be critical in determining the requirement of HB-EGF for cell growth. It was interesting that growth enhancement by HB-EGF was observed in reduced cell-matrix adhesion conditions, as seen in 2D-agar and NCPs, whereas HB-EGF-dependent cell growth was not observed in TCPs, which allow cells to attach, spread and form monolayers.

Growth rates of cells cultured in 3D or reduced cell adhesion conditions are much lower than those cultured in TCPs

To characterize the conditions that facilitate growth promotion by HB-EGF, we examined the growth rates of BRL cells under various culture conditions. For this experiment, methylcellulose gel was used instead of soft agar for the 3D-agar condition for the ease of cell counting (therefore referred to as 3D-MC). Since cell growth rate was different in each culture condition, cell number was counted at distinct culture periods. The growth curve of BRL-mock and BRL-HB cells in TCPs and 3D-COL are shown in Fig. 3A. Cell numbers of BRL-mock and BRL-HB cells cultured in NCP, 3D-LM, 2D-agar and 3D-MC for the days indicated are also shown in Fig. 3B. These results indicate that the growth rate of cells in TCPs is extremely high compared with that of other culture conditions in vitro. Based on Fig. 3A and 3B, we also examined the relationship of the 'growth rate' of BRL cells without HB-EGF and the 'upregulation ratio' by HB-EGF. The growth rate was estimated by comparison of the doubling time of BRL-mock cells in various culture conditions without HB-EGF, and the upregulation ratio was estimated by comparison of growth rate between BRL-mock and BRL-HB cells, as described in the Materials and Methods. Fig. 3C shows the relationship of the growth rate and upregulation ratio in each culture condition. The cells in culture conditions with lower growth rates showed a higher upregulation ratio, although this was not the case for 3D-MC. Thus, the enhancement of cell growth by HB-EGF was particularly observed in culture conditions in which overall cell growth was reduced.

HB-EGF enhances cell growth in 3D culture by activating Raf-MEK-Erk and PI3K-Akt pathways

We examined which EGFR downstream signaling molecules were responsible for cell growth in TCPs and 3D-COL upon HB-EGF stimulation. BRL-HB cell growth in 3D-COL was suppressed by inhibitors of EGFR (ZD1839), MEK (PD98059) and phosphatidylinositol-3 kinase (PI3K; LY294002), but not ErbB2

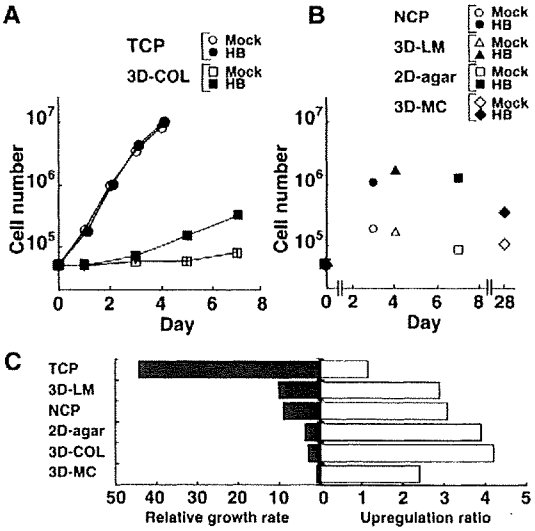

Fig. 3. Negative correlation between growth rate and HB-EGF dependency. (A) Growth curve of BRL cells (Mock) and BRL-HB cells (HB) in TCPs or 3D-COL. (B) Growth of BRL cells (Mock) and BRL-HB cells (HB) in NCP, 2D-agar, 3D-LM or 3D-MC. The numbers of cells was counted at indicated periods. (C) Relative growth rates and upregulation ratios under various culture conditions. Cell growth rates relative to that in 3D-MC and upregulation ratios by HB-EGF in various culture conditions.

(AG825) or p38MAPK (SB203580; Fig. 4A). This suggested that EGFR and its downstream MEK-Erk and PI3K-Akt signals were required for BRL-HB cell growth in 3D-COL. The PI3K inhibitor LY294002 inhibited BRL-HB cells in TCPs as well as in 3D-COL. Kinetic studies with increasing concentrations of inhibitors indicated that BRL-HB cell growth was largely suppressed by the MEK inhibitor PD98059 in 3D-COL and partially suppressed in TCPs within a higher concentration range (Fig. 4B). These findings suggest that MEK and PI3K are required for cell growth in TCPs as well as 3D-COL, but cells grown in 3D-COL were more susceptible to the inhibitors than cells grown in TCPs.

HB-EGF-dependent cell growth in 3D-COL was suppressed by inhibitors of MEK or PI3K, suggesting that activation of the Raf-MEK-Erk and PI3K-Akt pathways is crucial for promoting cell growth. To test whether activation of these pathways could substitute for the activity of HB-EGF, wild-type Raf-1, MEK1 and Akt1 were overexpressed in BRL-mock cells. Raf-1 alone, MEK1 alone or Raf-1 plus MEK1 did not significantly promote cell growth, whereas Akt1 alone partially promoted cell growth (data not shown). However, coexpression of Raf-1, MEK1 and Akt1, induced BRL cells to change their morphology to that resembling BRL-HB cells and promoted cell growth at comparable levels to those induced by HB-EGF (Fig. 4C), suggested that the coordinated activation of the Raf-MEK-Erk and PI3K-Akt pathways was crucial for potentiating cell growth in 3D-COL. By contrast, cell growth was not significantly affected by coexpression of Raf-1, MEK1 and Akt1 in TCPs (Fig. 4C). These results indicate that HB-EGF enhanced cell growth in 3D culture by activating both the Raf-MEK-Erk and PI3K-Akt pathways.

Attenuation of EGFR and its downstream signaling is associated with HB-EGF dependency

Next, we examined the activation states of EGFR, Erk and Akt in cells grown in TCPs and 3D-COL before and after transient HB-

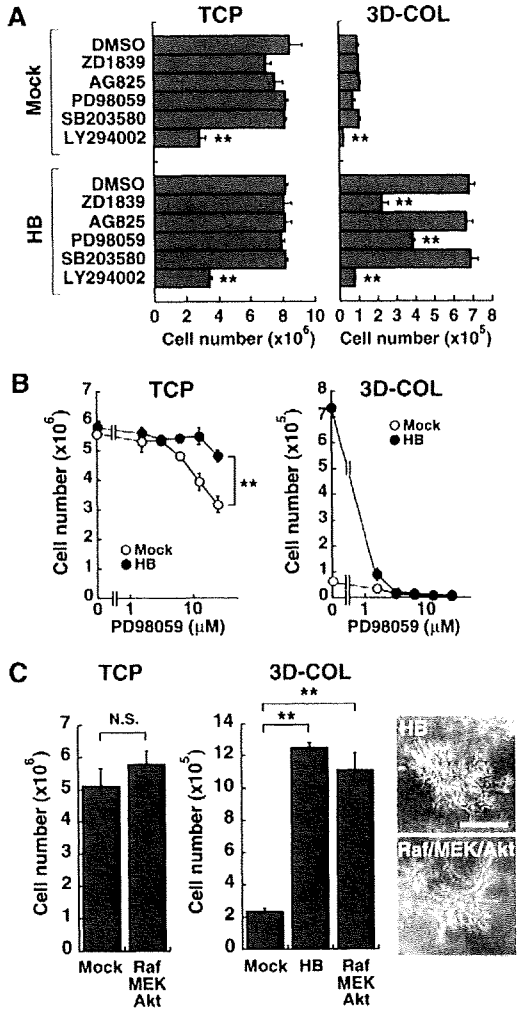

Fig. 4. Signaling pathways required for HB-EGF-dependent cell growth. (A) Effects of various kinase inhibitors on the growth of BRL cells. BRL-mock and BRL-HB cells were cultured in the presence of vehicle (DMSO) or the following kinase inhibitors: ZD1839 (100 nM), EGFR inhibitor; AG825 (100 nM), ErbB2 inhibitor; PD98059 (1 μM), MEK inhibitor; SB203580 (1 μM), p38MAPK inhibitor; or LY294002 (10 μM), PI3K inhibitor. (B) Effects of the MEK inhibitor on cell growth. Cells were grown in the presence of the indicated concentrations of PD98059. (C) Cooperation of Raf-1, MEK1 and Akt1. BRL-mock cells, BRL-HB cells or BRL cells expressing Raf-1, MEK1 and Akt1 were grown in TCPs for 4 days or 3D-COL for 1 week. Representative images of cells grown in 3D-COL are shown. All cell cultures were maintained in the presence of 10% FCS. N.S., not significant; $^{**}P<0.01$. Scale bar: 50 μm.

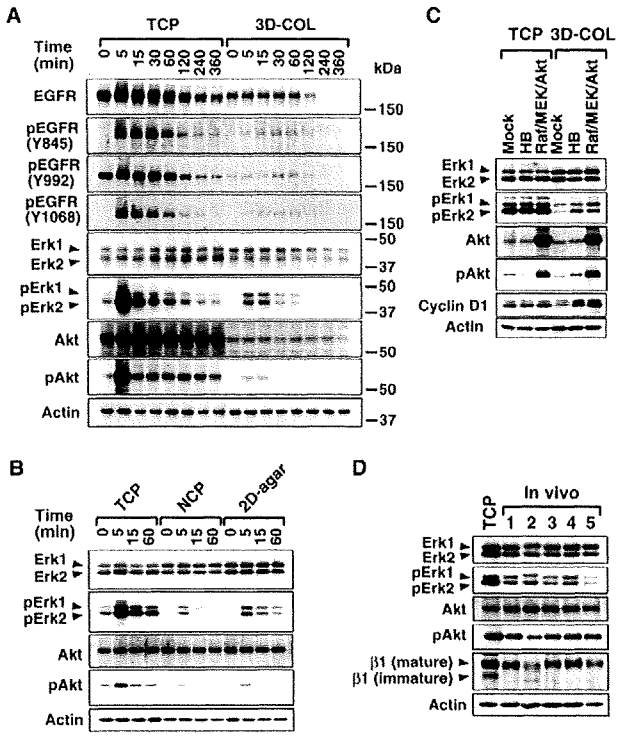

Fig. 5. Activation states of EGFR and its downstream pathways. (A) Transient activation of EGFR signaling in 3D-COL. BRL-mock cells were pre-cultured for 16 hours in the presence of 1% FCS in TCPs or 3D-COL, and then stimulated with recombinant sHB-EGF (30 ng/ml) for the indicated periods. Activation of EGFR, Erk and Akt was monitored using their phospho-specific antibodies. Actin was used as a control. (B) Transient activation of EGFR downstream pathways in 2D cell adhesion-reduced conditions. BRL-mock cells were pre-cultured for 16 hours in the presence of 1% FCS in NCPs or 2D-agar, and then stimulated with recombinant sHB-EGF (30 ng/ml) for the indicated periods. (C) Steady-state activation of EGFR downstream pathways. BRL-mock cells, BRL-HB cells and BRL cells expressing Raf-1, MEK1 and Akt1 were grown in TCPs or 3D-COL for 4 days in the presence of 10% FCS. Activation of Erk and Akt was monitored using their phospho-specific antibodies. Cell cycle was monitored with anti-cyclin-D1 antibody. Actin was used as a loading control. (D) Activation states of EGFR downstream pathways and the level of integrin β1 in vivo. BRL-HB cells were grown in TCPs for a day or nude mice for 3 weeks. Activation of Erk and Akt was monitored using their phospho-specific antibodies. Integrin β1 levels were monitored with anti-integrin β1 antibody. Actin was used as a control.

EGF stimulation. We first compared the steady-state levels of EGFR, Erk and Akt proteins of BRL cells cultured for 16 hours without sHB-EGF. The levels of EGFR and Akt proteins were markedly reduced in cells grown in 3D-COL compared with those grown in TCPs (Fig. 5A, see lanes Time 0). The Erk2, but not the Erk1 levels, were also slightly reduced in 3D-COL. Consistent with the reduction in the level of EGFR, the phosphorylation of EGFR (Y845 and Y992), Akt and Erk before HB-EGF stimulation was reduced in 3D-COL. These results indicate that the activation states of EGFR and downstream signaling molecules in the absence of HB-EGF in 3D-COL were lower compared with those in TCPs. Upon stimulation by addition of recombinant sHB-EGF, the phosphorylation levels of EGFR (Y845, Y992 and Y1068), Akt and Erk in TCPs were significantly enhanced. Although the phosphorylation levels of EGFR, Akt and Erk in 3D-COL were also enhanced by HB-EGF, they were much lower than those in TCPs (Fig. 5A).

The reduction of a cell response to HB-EGF in 3D-COL upon transient stimulation by sHB-EGF might be attributable to the reduced diffusion rate of sHB-EGF in the collagen gel. To test whether attenuation of EGFR signaling was characteristic of HB-EGF-dependent cell growth or due to the reduced diffusion, the activation states of Erk and Akt in cells grown in NCPs or 2D-agar were studied. In this case sHB-EGF would diffuse freely as it does in TCPs. Although Akt (Fig. 5B) or EGFR (data not shown) was

not reduced in NCPs or 2D-agar, steady states and sHB-EGF-induced phosphorylation levels of Erk and Akt in NCPs or 2D-agar were lower than those in TCPs, indicating that attenuation of EGFR signaling was not explained by the reduced diffusion rate of sHB-EGF (Fig. 5B).

Activation states of Erk and Akt were also examined under sustained cell culture conditions. For this assay, BRL-mock cells, BRL-HB cells and BRL cells expressing Raf-1, MEK1 and Akt1 were grown in TCPs or 3D-COL for 4 days in the presence of 10% FCS, and the phosphorylation levels of Erk and Akt were examined. The phosphorylation level of Erk in TCPs was much higher than that in 3D-COL regardless of the expression of HB-EGF or Raf-1, MEK1 and Akt1 (Fig. 5C). HB-EGF, or coexpression of Raf-1, MEK1 and Akt1, increased the phosphorylation level of Erk in 3D-COL, but the level was still lower than that of cells cultured in TCPs. This suggests a correlation between the phosphorylation level of Erk and the growth rate of BRL cells. The enhanced phosphorylation of Akt was also observed by expression of HB-EGF or coexpression of Raf-1, MEK1 and Akt1 in 3D-COL. This was consistent with results obtained using a transient assay (Fig. 5A), where expression of Erk and Akt in cells growing in 3D-COL was attenuated when compared with that in cells growing in TCPs. We observed that the phosphorylation level of Akt was reduced by expression of HB-EGF in TCPs, although the significance was not clarified.

We examined whether activation of the Raf-MEK-Erk and PI3K-Akt pathways is linked with cell cycle progression by evaluating cyclin D1 expression. BRL-mock cells showed reduced levels of cyclin D1 in 3D-COL compared with that in TCPs, suggesting that the cell cycle of BRL-mock cells in 3D-COL was arrested at G1 phase (Fig. 5C). Consistent with growth-promotion activity, HB-EGF or Raf, MEK and Akt increased cyclin D1 in 3D-COL to levels comparable with those in TCPs.

Finally, we examined EGFR downstream signaling in vivo. To determine the relationship of the activation state of EGFR signaling with HB-EGF dependency in cell growth, the phosphorylation levels of Erk and Akt of BRL-HB cells growing in tumors in mice were compared with those of BRL-HB cells growing in TCPs. The phosphorylation levels of Erk and Akt in tumors were lower than those of cells in TCPs (Fig. 5D), although the phosphorylation levels varied. Taken together, we conclude that the growth enhancement by HB-EGF was observed in culture conditions with lower levels of EGFR signaling compared with that seen in TCPs.

Integrin compensates for signals required for cell growth

Cell adhesion to the ECM substrate is mediated predominantly by integrins. Growth factor receptors and integrins activate some common signaling pathways (Schwartz and Ginsberg, 2002), and both signals cooperate functionally in a variety of biological processes. A previous study indicated that the expression level of EGFR is positively linked to that of integrin β1 and that both were crossregulated in 3D-LM (Wang et al., 1998). BRL cells mainly express β1 and β3 integrin subunits. Thus, we examined the levels of integrin β1 and integrin β3 proteins in BRL-mock cells grown in TCPs and 3D-COL. The integrin β1 levels in BRL-mock cells were significantly reduced when they were grown in 3D-COL compared with TCPs (Fig. 6A), whereas the levels of integrin β3 remained constant (data not shown). When HB-EGF was expressed in BRL cells, the level of integrin β1, particularly its mature form, was increased in cells grown in TCPs or 3D-COL. The combination of Raf-1 with MEK1 and Akt1 also consistently increased the integrin β1 levels under these culture conditions. We examined the level of integrin β1 of the BRL-HB cells growing in vivo and found that it was reduced in vivo compared with cells growing in TCPs (Fig. 5D). These results suggest that the integrin levels are linked with growth factor signaling in cells growing in 3D-COL or in vivo, as well as in 3D-LM.

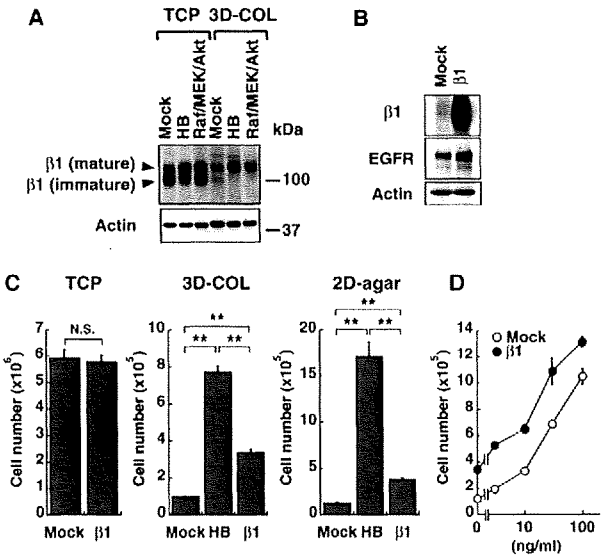

Fig. 6. Alteration of integrin β1 levels in various culture conditions. (A) Expression of integrin β1. BRL-mock cells, BRL-HB cells, or BRL cells expressing Raf-1, MEK1 and Akt1 were grown in TCPs or 3D-COL for 16 hours. The expression of integrin β1 was detected by immunoblotting. Actin was used as a loading control. (B) Expression of integrin β1 and EGFR in BRL-β1 cells. Expression of integrin β1 and EGFR in BRL-mock and BRL-β1 cells was detected using immunoblotting. Actin was used as a loading control. (C) Growth of BRL-β1 cells. BRL-mock, BRL-HB and BRL-β1 cells were cultured in TCPs for 4 days, in 3D-COL for 1 week or 2D-agar for 1 week. N.S., not significant; $^{**}P<0.01$. (D) Effect of recombinant sHB-EGF on growth of BRL-β1 cells. BRL-mock cells or BRL-β1 cells were cultured in 3D-COL for 1 week in the presence of indicated concentrations of recombinant sHB-EGF and 10% FCS.

To determine whether a reduced integrin β1 level in reduced cell adhesion conditions causes the diminished growth of BRL cells and their HB-EGF dependency, we established BRL cells expressing exogenous integrin β1 (BRL-β1) and examined cell growth in various culture conditions. Exogenous expression of integrin β1 resulted in an increased EGFR level (Fig. 6B). BRL-β1 cells grew faster than BRL-mock cells in 3D-COL or 2D-agar, but not in TCPs (Fig. 6C). However, cell growth rate induced by integrin β1 expression in 3D-COL or 2D-agar was slower than that induced by HB-EGF expression. Furthermore, when BRL-mock cells and BRL-β1 cells were stimulated with various concentrations of recombinant sHB-EGF in 3D-COL, BRL-β1 cells grew faster than BRL-mock cells in the same concentrations of sHB-EGF (Fig. 6D). However, the high concentration of sHB-EGF in BRL-mock cells far overcame the growth advantage of the BRL-β1 cells. These results suggest that a reduced integrin β1 level could partly cause the diminished growth of BRL cells and their HB-EGF dependency.

Integrins form stable focal contacts when cells are attached and spread to hard substrates, such as TCPs, with a corresponding

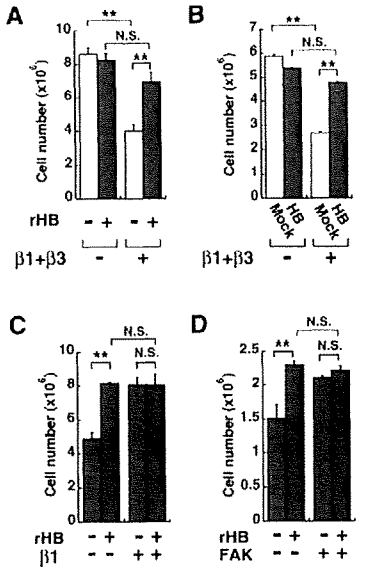

Fig. 7. HB-EGF dependency in cells cultured in reduced integrin conditions. (A) Effects of integrin antibodies on the growth of BRL cells in TCPs. BRL-mock cells stimulated with or without recombinant sHB-EGF (rHB; 30 ng/ml) were grown in the presence or absence of anti-integrin-β1 and anti-integrin-β3 antibodies (5 μg/ml each) in TCPs. (B) BRL-mock and BRL-HB cells were grown in the presence or absence of anti-integrin-β1 and anti-integrin-β3 antibodies (5 μg/ml each). (C) Effect of recombinant sHB-EGF on growth of integrin-β1-knockout cells in TCPs. Integrin-β1-knockout cells or integrin-β1-knockout cells expressing integrin β1 were cultured in the presence or absence of recombinant sHB-EGF (rHB; 30 ng/ml) in TCPs. (D) Effect of recombinant sHB-EGF on growth of FAK-knockout cells in TCPs. FAK-knockout cells or FAK-knockout cells expressing FAK were cultured in the presence or absence of recombinant sHB-EGF (rHB; 30 ng/ml) in TCPs. These cultures were maintained in the presence of 10% FCS. N.S., not significant; $^{**}P<0.01$.

generation of strong signals. By contrast, when cells are cultured on soft substrates, the formation of focal contacts is hampered, and integrin signals are reduced (Cukierman et al., 2001; Paszek et al., 2005). Although it is difficult to accurately estimate the strength of integrin signals directly, the morphology of cells cultured under various conditions (Fig. 2) and the phosphorylation levels of Erk and Akt in the absence of HB-EGF (Fig. 5) represent the strength of integrin signals within a particular cell culture system. Therefore, we speculated that, in combination with the expression level of integrin β1, integrin signals are strengthened in TCPs, whereas they are considerably decreased in 3D or 2D adhesion-reduced culture conditions.

We hypothesized that the integrin signal might predominantly contribute to promote cell growth in TCPs, thereby allowing the cells to grow without HB-EGF. However, integrin signals were too low to grow in cells cultured in 3D and 2D adhesion-reduced conditions, resulting in enhanced cell proliferation by HB-EGF. To test this hypothesis, we investigated the effect of integrin inhibition on HB-EGF dependency for cell growth in TCPs. First, BRL cells were cultured in the presence or absence of integrin antibodies. Although a single blockade of integrin β1 or integrin β3 scarcely inhibited the growth of BRL cells (data not shown), simultaneous blockade of integrins β1 and β3 suppressed the growth of BRL cells in TCPs (Fig. 7A). When sHB-EGF was added to the culture with the integrin antibodies, sHB-EGF almost recovered the growth rate to the level of BRL cells without the integrin antibodies, indicating that BRL cells exhibit HB-EGF-dependent growth in the presence of integrin antibodies. Growth stimulation by HB-EGF in TCPs was also shown upon comparison of the growth rate of BRL-mock and BRL-HB cells in the presence of integrin antibodies (Fig. 7B).

To further examine the contribution of integrin to cell growth in TCPs, we examined the HB-EGF dependency of cells obtained from an integrin-β1-knockout mouse. Fig. 7C shows that growth of cells lacking integrin β1 was HB-EGF-dependent in TCPs. Growth stimulation of integrin-β1-knockout cells was observed by addition of sHB-EGF to the medium. Reintroduction of integrin β1 increased the growth of integrin-β1-knockout cells in TCPs and induced the cells to become HB-EGF independent. These results indicate that the integrin system largely contributes to the growth of cells cultured in TCPs. FAK is a critical downstream effector of integrin signaling (Mitra and Schlaepfer, 2006). To further strengthen our hypothesis, we examined whether fibroblasts obtained from FAK-knockout mice ($MEF^{FAK-/-}$) showed HB-EGF dependency for growth in TCPs. Similarly to cases of integrin blockade with integrin antibodies (Fig. 7A,B) and integrin-β1-knockout cells (Fig. 7C), $MEF^{FAK-/-}$ cells exhibited HB-EGF-dependent growth in TCPs upon addition of sHB-EGF to the medium (Fig. 7D). Reintroduction of FAK increased the growth of FAK-knockout cells in TCPs, and the cells became less HB-EGF independent. Taken together, we conclude that integrin and HB-EGF share common signals for promoting cell growth, and that in TCPs integrins generate sufficient signals for growth, thereby contributing to the dispensability of HB-EGF for growth purposes. In 3D or 2D adhesion-reduced conditions the integrin signals are not sufficient to stimulate rapid cell growth, and therefore there is a cumulative contribution of integrins and growth factors toward cell growth.

3D culture facilitates growth-stimulatory activity of EGF, TGFα or ligands of other RTKs

We demonstrated here that growth stimulation by HB-EGF was facilitated in 3D culture systems or 2D cell adhesion-reduced conditions. To determine whether this feature was specific for HB-EGF or was a general feature of other growth factors, we tested the growth-stimulatory effects of various growth factors in TCPs and 3D-COL. None of the growth factors tested greatly enhanced cell growth of BRL-mock cells in TCPs. EGF and TGFα of the EGF family enhanced cell growth to the same extent as HB-EGF did in 3D-COL (Fig. 8). In addition, the growth of BRL cells in 3D-COL was enhanced by FGF-2 and IGF-1 and slightly enhanced by PDGF-BB (Fig. 8). These results indicate that culture conditions with reduced integrin signals also facilitated cell growth promotion by other members of the EGF family of growth factors or ligands of other RTKs.

Discussion

In this study, SKOV3 and BRL cells injected into nude mice exhibited HB-EGF-dependent growth; however, when these cells were cultured in TCPs, they displayed no HB-EGF dependency. Based on this finding, we investigated the effects of HB-EGF on cell growth under different culture conditions. Our results indicated the following: first, the HB-EGF dependency of cell growth was emphasized in culture systems in which cells grew in reduced cell-substrate adhesion, and this phenomenon was observed for transformed and non-transformed cells; second, the phosphorylation